Supplementary Materials

Living Nanospear for Near-Field Optical Probing

Yuchao Li[1], Hongbao Xin[1], Yao Zhang[1], Hongxiang Lei[2], Tianhang Zhang[3,4], Huapeng Ye[4], Juan Jose Saenz[5,6], Cheng-Wei Qiu[3,4] & Baojun Li[1]**

[1]Institute of Nanophotonics, Jinan University, Guangzhou 511443, China.

[2]School of Materials Science and Engineering, Sun Yat-Sen University, Guangzhou, 510275, China.

[3]Graduate School for Integrative Sciences and Engineering, National University of Singapore, Centre for Life Sciences (CeLS), #05-01, 28 Medical Drive Singapore 117456, Singapore

[4]Department of Electrical and Computer Engineering, National University of Singapore, Singapore 117583, Singapore.

[5]Donostia International Physics Center (DIPC), Paseo Manuel de Lardizabal 4, Donostia-San Sebastian 20018, Spain.

[6]IKERBASQUE, Basque Foundation for Science, 48013 Bilbao, Spain.

[*]Address correspondence to baojunli@jnu.edu.cn and eleqc@nus.edu.sg.

1. Experimental Set-Up

The experimental set-up is shown in Fig. S1. The experiments were performed on an optical microscope with a ×100 objective (numerical aperture: 0.9) in transmission mode. The microscope was interfaced with a charge coupled device (CCD) (DXC-S500, Sony iCY-SHOT), which was linked to a personal computer (PC) to observe the experimental process. Two fibers (input and output fiber), sheathed with glass capillaries, were mounted on tunable three-axis micromanipulators (Kohzu Precision Co., Ltd., precision: 50 nm) in opposite directions. The tips of the fibers were inserted into a microfluidic channel (length: 2.0 cm, width: 800 μm, depth: 800 μm) which contained the suspensions of experimental samples and was placed on a translation stage. The tail end of the input fiber was connected to the stem of a 1 × 4 fiber coupler. Input lasers were connected to two arms of the fiber coupler and supplied continuous-wave laser beams into the input fiber with different wavelengths for implementing different functions. Specifically, near-infrared laser (808 nm) was used for trapping biological cells, visible lasers (644, 532, and 473 nm) were applied for bio-nanospear illumination, and ultraviolet laser (390 nm) was employed for exciting the fluorescence. The other two arms of the fiber coupler were connected to an InGaAs photodetector (PD) (bandwidth: 1.2 GHz, bandpass: 790–1200 nm, DET01CFC, Thorlabs), and a spectrometer (grating density: 900 grooves/mm, bandpass: 400–650 nm, QE65 Pro, Ocean Optics) for monitoring the 808-nm backscattering signal and measuring the fluorescence signal,

respectively.

To measure the optical power output from the bio-nanospear, the tapered tip of the output fiber was connected to the end of the bio-nanospear, and then the tail end of the output fiber was connected to an optical power meter (OMM-6810B, ILX Lightwave). Noted that the 808-nm trapping laser remained on in the experiments to keep the stability of the bio-nanospear. To minimize the influence of the 808-nm laser beam when measuring the optical powers of other wavelengths, a fiber band-stop filter (MP-808-HR-GA, Micro Photons Technology Co., Ltd.) with a central wavelength of 808 nm was linked to the optical power meter.

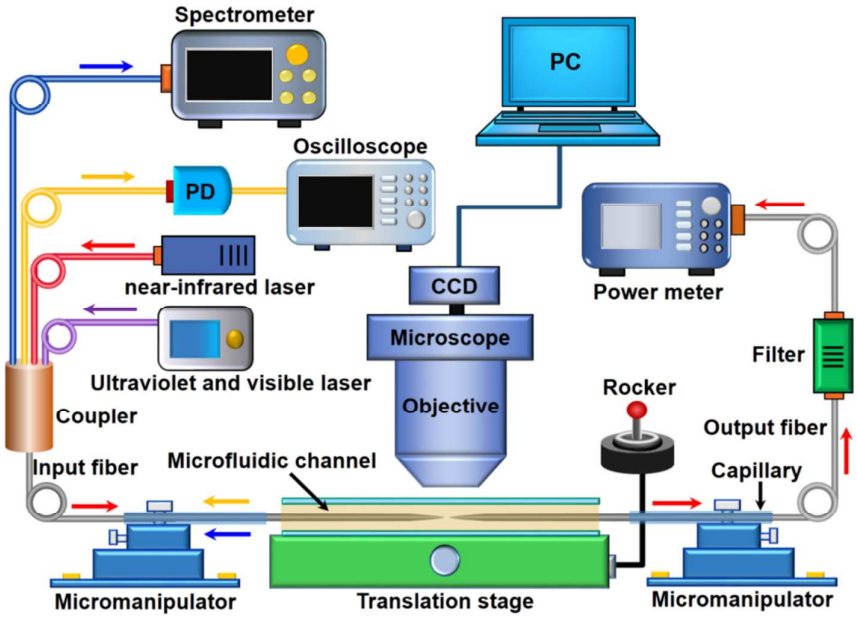

Figure S1 | Schematic of the experimental set-up. The red, purple, blue and yellow arrows indicate the propagation of the trapping laser (808 nm), illumination laser (including 390, 473, 532 and 644 nm), fluorescent signal (510 nm) and backscattering signal (808 nm), respectively. The input fiber was used to manipulate the bio-nanospear, transmit the input lasers and collect the optical signals, while the output fiber was used to measure optical power output from the bio-nanospear. CCD, charge-coupled device; PD, photodetector; PC, personal computer.

2. Simulation and Calculation of the Orientation of the *L. acidophilus*

To determine the stable orientation of the *L. acidophilus* cell, a finite element method was used to simulate and calculate optical torque T exerting on the *L. acidophilus* cell. The geometry of the yeast and *L. acidophilus* cell was assumed to be a dielectric sphere (radius: 1.4 μm) and nanocapsule (length: 2.0 μm; radius: 200 nm) with hemispherical caps, respectively. The geometrical parameters were obtained by choosing 100 yeast and *L. acidophilus* cells randomly from scanning electron microscope images and calculating the average values of their radius and length. To acquire a suitable computational accuracy and efficiency, the mesh sizes of the regions of the yeast and *L. acidophilus* cells were set as 30 and 50 nm, respectively, and the corresponding refractive indices were set as 1.39 and 1.40, respectively. Fig. S2a–d shows the simulated energy density distributions of the 808-nm

trapping laser beam when a *L. acidophilus* cell was positioned in the output light spot with different azimuthal angle θ (the angle between the optical axis and the long axis of the *L. acidophilus* cell). The torque T of the *L. acidophilus* cell can be calculated by[1,2]

$$\mathbf{T} = \int \mathbf{r}_p \times d\mathbf{F}_p , \tag{S1}$$

where $d\mathbf{F}_p$ is the optical force element at the interaction point p, and $\mathbf{r}_p$ is the position vector pointing from the central point of the *L. acidophilus* cell to the interaction point. As a result, Fig. S2e shows the calculated T acting on the *L. acidophilus* cell as a function of θ (black-dotted curve). By integrating the values of T with respect to θ, the rotational potential energy U of the *L. acidophilus* cell can be obtained, as shown in Fig. S2e (red-dotted curve). It can be seen that the rotational potential energy U reaches the minimum at $\theta = 0$, which demonstrates that the most stable orientation for the trapped *L. acidophilus* cell is $\theta = 0$.

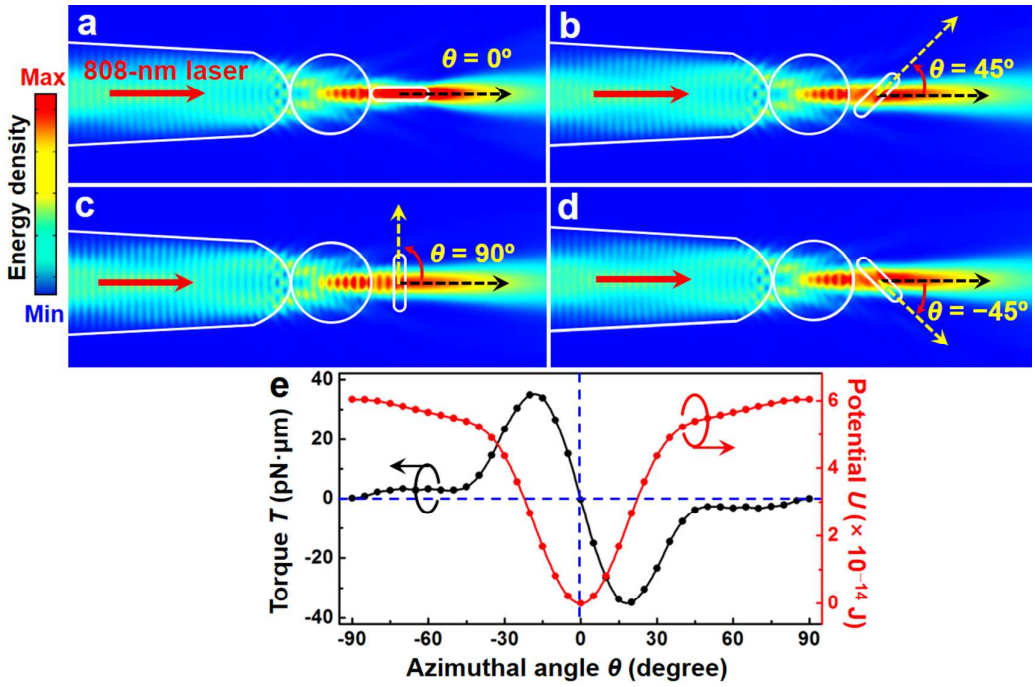

Figure S2 | Simulation and calculation of the orientation of the trapped *L. acidophilus* cell. a–d, Simulated energy density distributions of the 808-nm trapping laser beam when a *L. acidophilus* cell was located in the output light spot with azimuthal angle θ of 0^o (a), 45^o (b), 90^o (c), and -45^o (d). The input optical power of the 808-nm laser was normalized to be 1 W. e, Calculated optical torque T (black-dotted curve) and rotational potential energy U (red-dotted curve) of the trapped *L. acidophilus* cell as a function of θ.

3. Trapping Stiffness and Optical Force of the Cells in the Nanospear

By tracking the thermal fluctuations of the cells (at a trapping power of 15 mW) in time with a high-speed video microscopy (Fig. S3a1–g1), and then fitting the fluctuation distributions with Gaussian models (Fig. S3a2–g2), the standard deviations σ of the Brownian fluctuation for the yeast cell and six *L. acidophilus* cells in the y direction were obtained as 9.8, 6.6, 5.8,

6.0, 6.6, 7.0, and 7.3 nm, respectively (Fig. S3h). The Gaussian distributions of the Brownian fluctuations indicate that the cells were trapped in harmonic potential wells. For this situation, the trapping stiffness κ of the cells can be obtained from the equipartition theorem:[3]

$$\kappa = \frac{k_B T}{\sigma^2} \quad , \tag{S2}$$

where k_B is Boltzmann's constant, T is the absolute temperature of the medium, and σ is the standard deviation of the Brownian fluctuation of the cells. From equation (S2), the values of κ for the yeast cell and six *L. acidophilus* cells were calculated as 4.3, 9.5, 12.3, 11.5, 9.5, 8.4, and 7.8 × 10^{-2} pN/nm, respectively. After the determination of κ, the optical forces F can be obtained from

$$F = \kappa \cdot q \quad , \tag{S3}$$

where q is the positional coordinate of the cells.

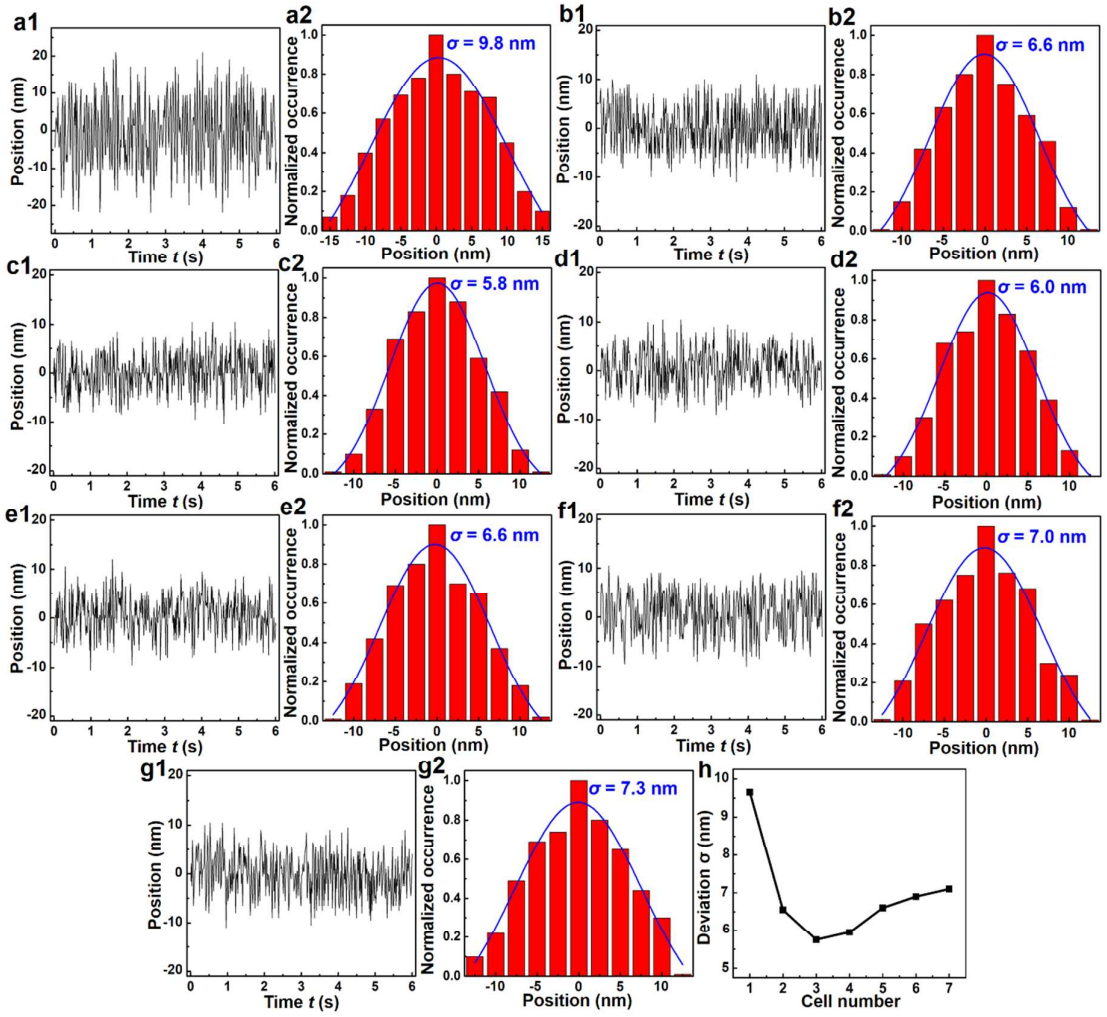

Figure S3 | Brownian fluctuation and trapping stiffness of the nanospear. a1–g1, Real-time trace of the thermal fluctuations of the yeast cell and six *L. acidophilus* cells at a trapping power of 15 mW. a2–g2, The histograms of the fluctuation distributions for the yeast

cell and six *L. acidophilus* cells with Gaussian fittings. h, The standard deviations σ of the Brownian fluctuation as a function of cell number in the nanospear.

4. Frequency-Domain Analysis of the Backscattering Signal

The trapping stiffness κ can be also calculated by using the backscattered light at 808 nm from the cells (Fig. S4a) to perform a frequency-domain analysis of the thermal fluctuations of the cells. In this method, κ is expressed as[4]

$$\kappa = 2\pi\beta f_c \ , \tag{S4}$$

where f_c is the corner frequency of a Lorentzian model fitted to the power spectral density of the fluctuation distribution, and β is the Stokes drag on cells, which is expressed as

$$\beta = 6\pi\eta r \ , \tag{S5}$$

where η is the viscosity of the medium and r the radius of the yeast cell. The power spectral density $P(f)$ can be fitted by the Lorentzian model with the following form[5]

$$P(f) = \frac{k_B T}{\pi^2 \beta (f^2 + f_c^2)} \ . \tag{S6}$$

Here, we performed the frequency-domain analysis for the yeast cell as an example (Fig. S4b). From the Lorentzian fitting of the power spectral density of the yeast cell, the corner frequency f_c was obtained as 340 Hz. Therefore, the trapping stiffness κ was calculated as 4.1 $\times$ 10^{-2} pN/nm, which agrees with the value of 4.3 $\times$ 10^{-2} pN/nm measured by the video microscopy method.

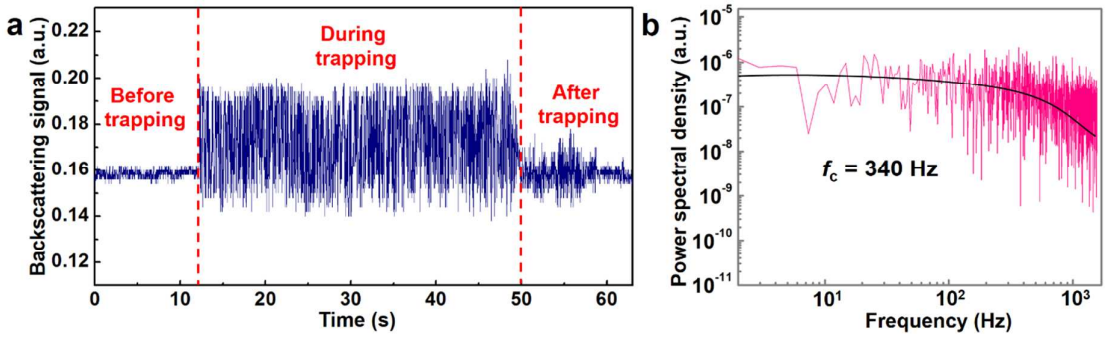

Figure S4 | Frequency-domain analysis of the backscattering signal. a, The real-time trace of the backscattering signal at 808 nm in the trapping process of a yeast cell. b, Power spectral density calculated from the backscattering trace and the fitted curve (black) to the Lorentzian model with a corner frequency of f_c = 340 Hz.

5. Light Propagation of the Nanospear and Tapered Fibers with a Subwavelength Tip

Figures S5a–d present the simulated energy density distributions of the 808-nm propagating light through the bio-nanospear and tapered fibers with a subwavelength tip. In the simulation, the refractive index of the cell chain in the bio-nanospear and fiber tips was set as 1.40. The results show that the incident light can effectively propagate along the cell chain output a tiny light spot at the end. However, for the fiber tips with diameters of 400 and 100 nm, a large

part of the evanescent wave diverges into the water and then loses in the far field, which generates relatively large light spots (Fig. S5e–h). Thus, the fiber nano-tips cannot yield any subwavelength imaging capacity. Additionally, the simulated energy density distribution shows that the output light spot from the 400 nm fiber tip with a yeast cell is larger than that of the nanospear with a cell chain. Besides, the evanescent field of the nanospear with a cell chain is narrow than that of the 400 nm fiber tip with a yeast cell. Therefore, the cell chain instead of the yeast cell is the main advantage of the optical properties of the nanospear.

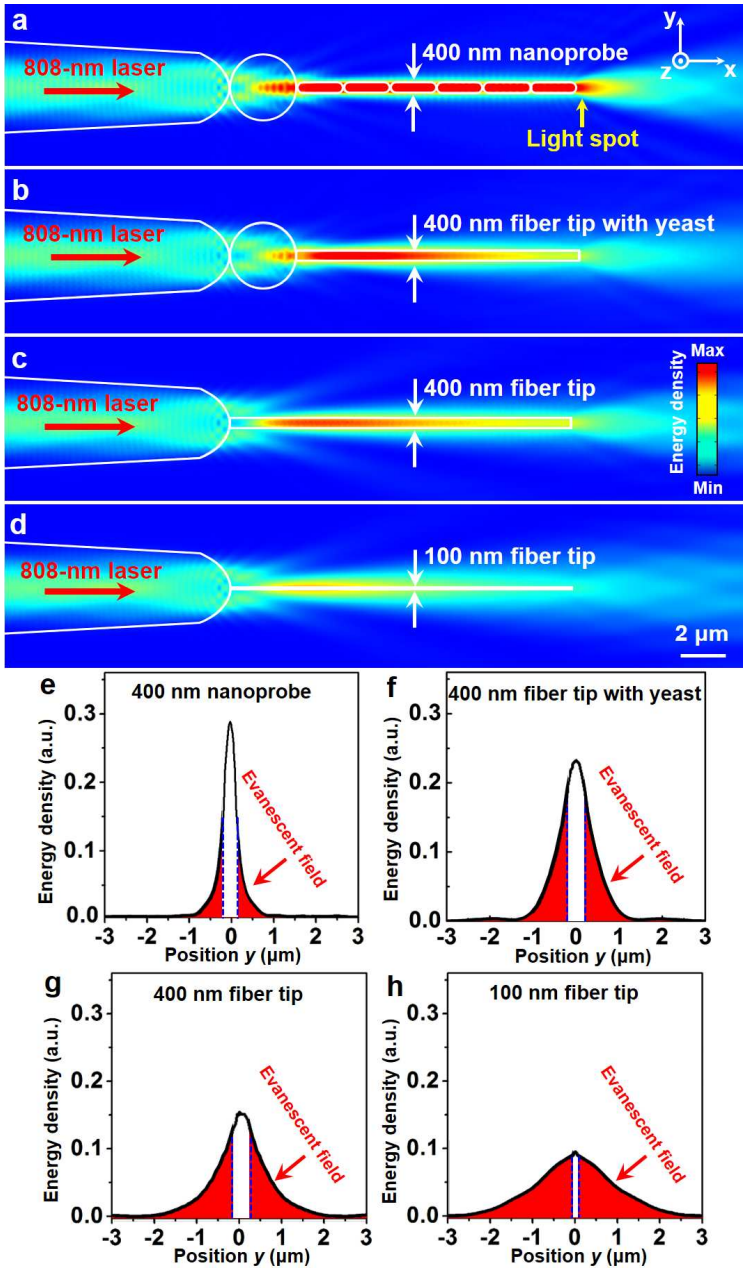

Figure S5 | Light propagation of the nanospear and tapered fibers with a subwavelength tip. a–d, Simulated energy density distributions of the 808-nm propagating light through a nanospear (a), a 400 nm fiber tip with a yeast cell (b), a bare 400 nm fiber tip (c), and a 100 nm fiber tip (d). e–h, Energy density profiles of the propagating light along a nanospear (e), a

400 nm fiber tip with a yeast cell (f), a bare 400 nm fiber tip (g), and a 100 nm fiber tip (h). in the *y* direction. The red-filled areas indicate the evanescent fields outside the nanospear and fiber tips.

6. Light Spot of a Single *L. acidophilus* Cell

Figures S6a and b present the dark-field microscope image and simulated energy density distribution of the scattering light spot with 644 nm wavelength from a single *L. acidophilus* cell. For comparison, the *L. acidophilus* cell was located at the same position as the last cell of the cell chain and the optical power of the input laser was set as the same as the previous experiments and simulations. The result of Fig. S6c shows that, the optical intensity of the light spot from the cell chain (1.00) is approximately three times higher than that of the single cell (0.33), which verifies the sub-wavelength focusing effect of the nanospear is attributed to the multiple focusing effect of the cell chain instead of the single cell.

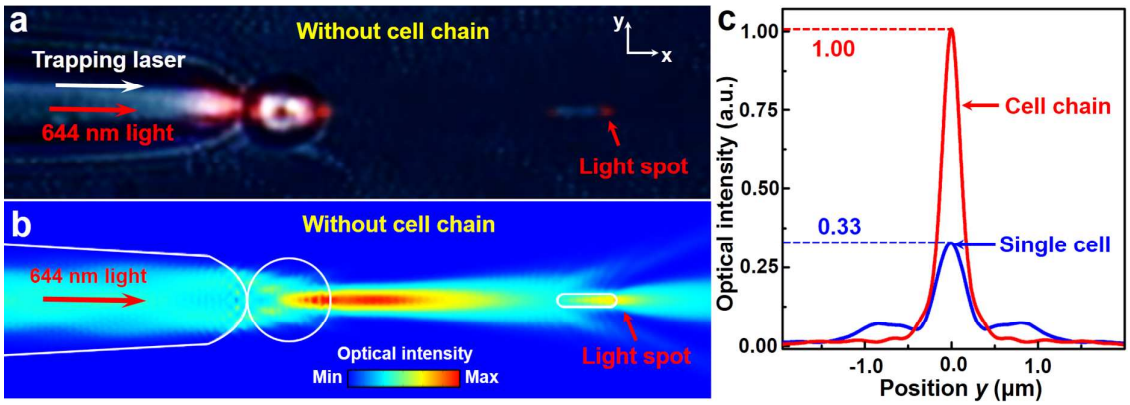

Figure S6 | Scattering light spot from a single *L. acidophilus* cell. a,b, Dark-field microscope image (a) and simulated energy density distribution (b) show the scattering light spot with 644 nm wavelength from a single *L. acidophilus* cell. c, Normalized optical intensity profiles at the focal planes of the output light spots of the cell chain in the nanospear (red line) and a single cell (blue line) in the *y* direction.

7. Light Spot Size of the Nanospear *versus* the Cell Number and Chain Length

Additional experiments and simulations were performed to characterize how the spot size changes with the number (*N*) of *L. acidophilus* cells and the chain length (*L*). Dark-field images in Fig. S7a–c show the output light spots of 532 nm illumination from the nanospears with the cell number *N* of 3, 7 and 11, respectively (the corresponding chain length *L* were 6.0, 15.6 and 23.5 μm, respectively). Figure S7d–f show the simulated energy density distributions of the output light spots from the nanospear with the same cell number as the experiments. The light spot size was measured by performing the line scans through the output light spots in the vertical direction using MATLAB software. The experimental results (red lines in Fig. S7g and h) show that the light spot size of the illumination light varies from 282 to 340 nm (variation rate: 0.21) when the cell number ranges from 1 to 13 (chain length: 2 to 29 μm). For comparison, theoretical simulations (black lines in Fig. S7g and h) indicate that the light spot size changes from 280 to 330 nm (variation rate: 0.18) when the cell number increases from 1 to 13 (chain length: 2 to 26 μm). Therefore, the theoretical simulations agree with the

experimental results.

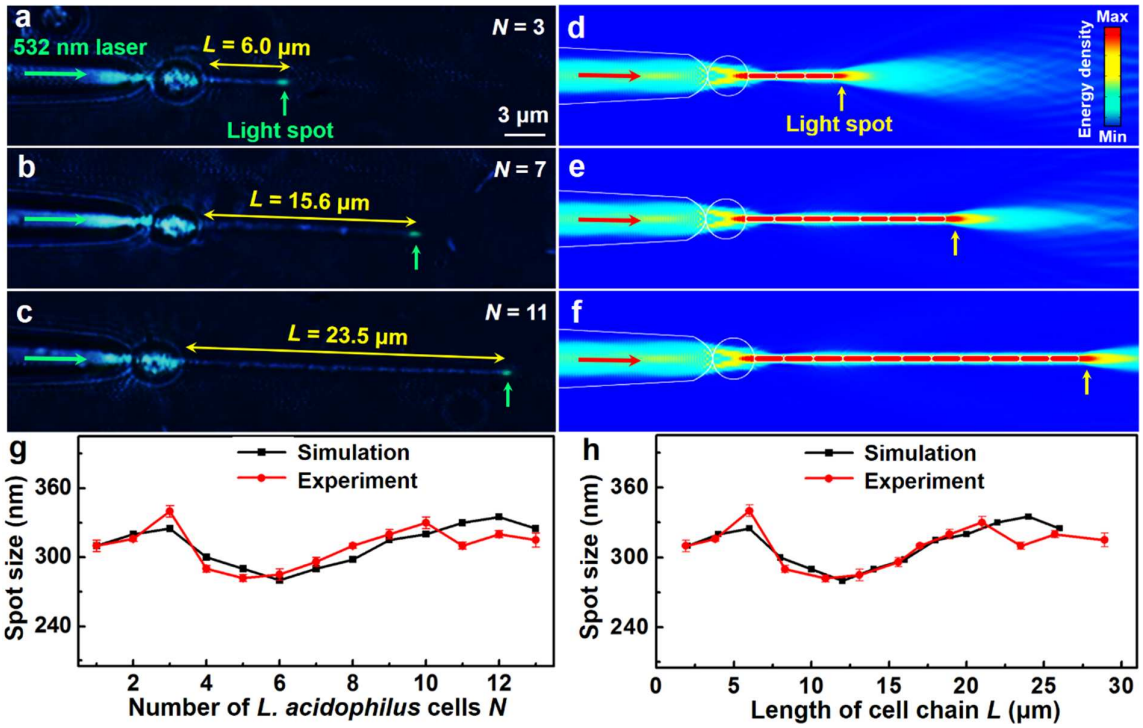

Figure S7 | Light spot size of the nanospear *versus* the cell number and chain length. a–c, Dark-field images indicate the 532-nm illumination light propagating along the nanospears with cell number N of 3 (a), 7 (b), and 11 (c). d–f, Simulated energy density distributions of the 532-nm illumination light propagating along the nanospears with cell number N of 3 (d), 7 (e), and 11 (f). g, The interplay between the cell number N and light spot size. h, The interplay between the chain length L and light spot size. Black line: simulation; Red line: experiment.

8. Fluorescence Resolution and Brownian Fluctuation *versus* Trapping Power

When the trapping powers were set as 5, 10, 12, 15, and 20 mW, the values of the fluorescence resolution were measured as 262, 254, 218, 220, and 248 nm, respectively (Fig. S8a). Therefore, the resolution discrepancies $|\Delta R|$ between the fluorescence resolution R_{fluo} and actual resolution R_{SEM} (235 nm) obtained by the SEM image were 27, 19, 17, 15 and 13 nm, respectively. By using video tracking method, the lateral Brownian fluctuations σ of the nanospear end were recorded as 13.6, 9.2, 8.1, 7.3 and 6.4 nm at trapping powers of 5, 10, 12, 15 and 20 mW, respectively. From the comparison of σ and $|\Delta R|$ (Fig. S8b), it can be found that the values of 2σ approximately equal to $|\Delta R|$. Therefore, the measured fluorescence resolution R_{fluo} can be corrected by $R_{\text{fluo}} = R_{\text{SEM}} \pm 2\sigma$.

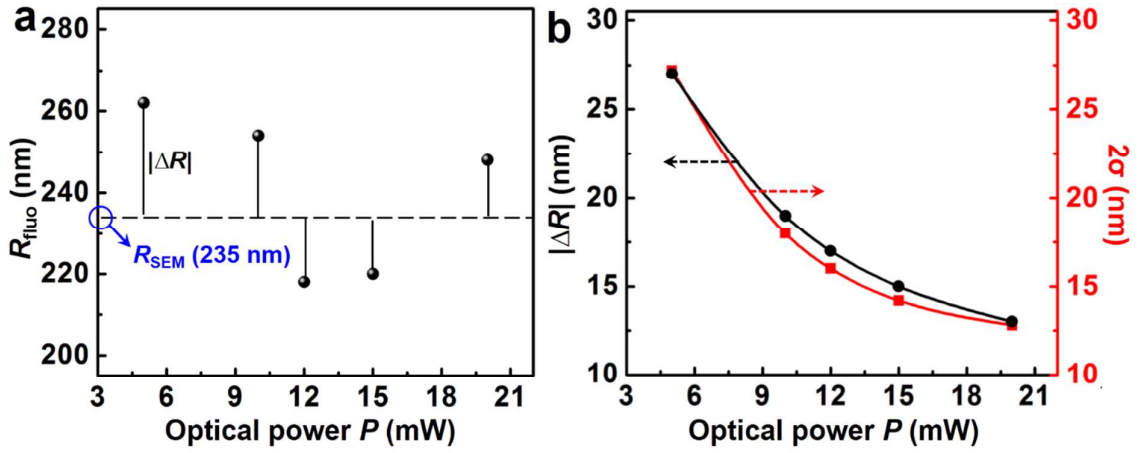

Figure S8 | Fluorescence resolution and Brownian fluctuation *versus* trapping power. a, The measured fluorescence resolutions R_{fluo} as a function of trapping powers P. R_{SEM} represents the actual resolution (235 nm) obtained from the SEM image and $|\Delta R|$ is the resolution discrepancies $|\Delta R|$ between R_{fluo} and R_{SEM}. b, The resolution discrepancies $|\Delta R|$ and two times of Brownian fluctuations 2σ as a function of trapping powers P.

9. Detection and Scanning of a Single Cancer Cell in a Microfluidic Capillary

To further investigate the scanning capabilities of the nanospear, we have applied this scanning approach to a simulated blood capillary system, which was composed of a polymer micro-capillary (inner diameter: 15 μm; length: 1.0 cm) and a micro-pump system (KDS LEGATO 270). The experimental configuration is schematically shown in Fig. S9a. Two optical fiber probes (marked as fiber 1 and fiber 2) were oppositely inserted into the micro-capillary for the uses of assembling the nanospear and trapping the samples, respectively. A flowing suspension (flow velocity: 35 μm/s) that contains *L. acidophilus* cells, yeast cells, red blood cells and fluorescent cancer cells (K562) was injected into the micro-capillary through the micro-pump system with a push-pull configuration. To generate stable optical traps in the flow, two trapping lasers at 808 nm wavelength with optical powers of 30 and 60 mW were launched into the fiber 1 and 2, respectively. By controllably manipulating the fibers in the micro-capillary, a yeast cell and five *L. acidophilus* cells were orderly assembled at the tip of the fiber 1, and a fluorescent cancer cell was stably trapped by the fiber 2 as the sample to be scanned. To avoid trapping other cells and objects during the scanning process, the backscattering signal of the 808-nm trapping laser was detected in real-time. To excite the fluorescence from the cancer cell, an ultraviolet light at 390 nm wavelength with an optical power of 100 μW was sent to the fiber 1. Then the nanospear was moved to contact the cancer cell for exciting and detecting the localized fluorescence from the cell surface. By precisely moving the nanospear with the fiber 1, the surface of the cancer cell can be scanned at different positions, as shown in Fig. S9b–d.

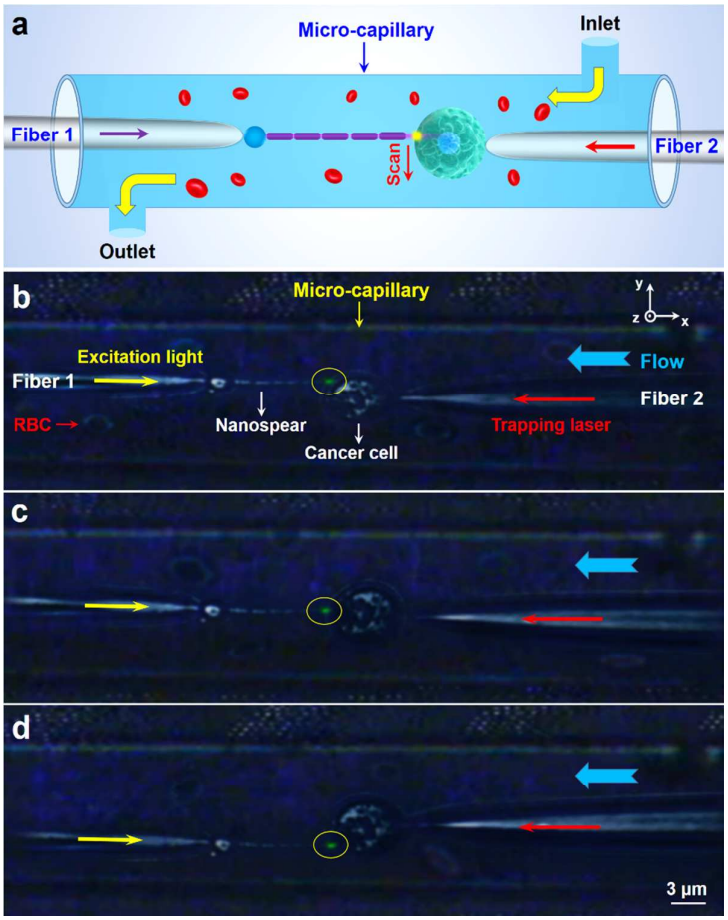

Figure S9 | Detection of localized fluorescence from a single cancer cell in a micro-capillary. a, Schematic illustrating the experimental configuration. Two optical fiber probes (marked as fiber 1 and fiber 2) were oppositely inserted into the micro-capillary for assembling the nanospear and trapping the cancer cells, respectively. b–d, Dark-field optical images showing the excitation and detection of the localized fluorescence from a trapped cancer cell by manipulating the nanospear to scan the cell surface at different locations.

10. Morphological Scan of a Single Fluorescent Micro-Bead

To demonstrate the morphological scan ability of the nanospear, a fluorescent polystyrene micro-bead with a diameter of 6 μm was selected as a scanning sample. To reduce the influence of Brownian motion, the micro-bead was rigidly adhered to a glass substrate. Fluorescence and SEM images (Fig. S10a and b) show that the micro-bead has a uniform fluorescence distribution and regular spherical shape. To simplify the experiment, we performed the morphological scan at a portion of the micro-bead surface in a two dimensional (2D) plane (*x*-*y* plane). The full 3D surface scan can be achieved by moving the nanospear in the *z* direction and rotating the nanospear with precise orientations. The process of the morphological scan is as follows. First, the nanospear was assembled at the desired position alongside the micro-bead. To maximize scanning speed, the nanospear was controlled to approach the micro-bead with 500-nm steps in the *x* direction, and then was finely adjusted with 50-nm steps (Step 1), as schematically shown in Fig. S10c. The distance between the

nanospear and the sample was controlled by monitoring the fluorescence intensity from the micro-bead (Fig. S10d). When the fluorescence intensity reaches the nominated threshold, the positional coordinate of the largest intensity of the fluorescent spot was defined as a pixel point (x_i, y_i). To reduce the influence of the nanospear's Brownian fluctuation, the pixel point is an average of three consecutively recorded images. After the fluorescence intensity exceeds the fluorescence threshold, the nanospear was retracted to the initial position (Step 2), and then was moved in the y direction with a 100-nm step to start the scan for next pixel point (Step 3), as schematically shown in Fig. S10e. After finishing the scanning, a 2D surface morphology of the micro-bead can be reconstructed in post-processing by superimposing the scanning pixel points in an image. As shown in Fig. S10f, the black dots represent the positional coordinate points of the scanning pixels and the background sphere indicates the position of the fluorescent micro-bead. This preliminary experiment demonstrates that the nanospear can be applied for combining fluorescence with a morphological scan.

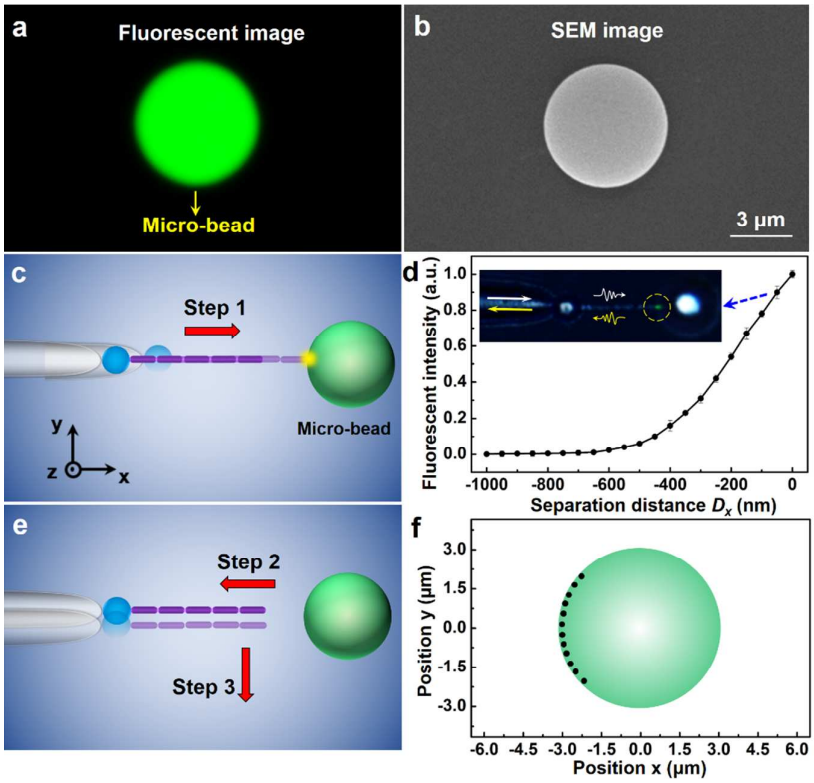

Figure S10 | Morphological scan of a fluorescent micro-bead. a, Fluorescence image shows the green fluorescent light from a single polystyrene micro-bead with a diameter of 6 μm. b, Corresponding SEM image showing the micro-bead has a regular spherical shape. c, Schematics showing the nanospear is positioned alongside the micro-bead and then is advanced in a stepwise manner until the fluorescent intensity reaches the threshold value (Step 1). d, The fluorescent intensity as a function of the separation distance between the tip of the nanospear and the surface of the micro-bead. The inset shows the dark-field images of the nanospear with a separation distance of 50 nm from the micro-bead. e, Schematics showing the nanospear is drew back to its original position (Step 2), and then moved to the next pixel's starting location (Step 3). f, A two dimensional surface morphology of the micro-bead by superimposing the pixel points in an image. The black dots represent the

positional coordinate points of the scanning pixels. The background sphere indicates the position of the fluorescent micro-bead.

11. Optical manipulation of a single cell using the nanospear

An experiment demonstrated that the nanospear can be used for flexible manipulation of single biological cells. As shown in Fig. S11a, a *Staphylococcus aureus* (*S. aureus*) cell dyed with green fluorescence protein was trapped at the tip of the nanospear. Then by moving the nanospear in the $-x$ direction with an average velocity of 26 μm/s, the trapped *S. aureus* cell was simultaneously moved with a distance of 8 μm (Fig. S11b) and 16 μm (Fig. S11c) at t_1 = 0.3 s and 0.6 s, respectively. The formed nanospear kept stable during the manipulation process. Similarly, the trapped cell can be also moved in the $-y$ direction by manipulating the nanospear. As shown in Fig. S11d and e, the trapped *S. aureus* cell was moved with a distance of 8 μm at t_2 = 0.3 s. This experiment indicates that the nanospear constructed with soft materials can also find applications in the manipulation of biospecimens.

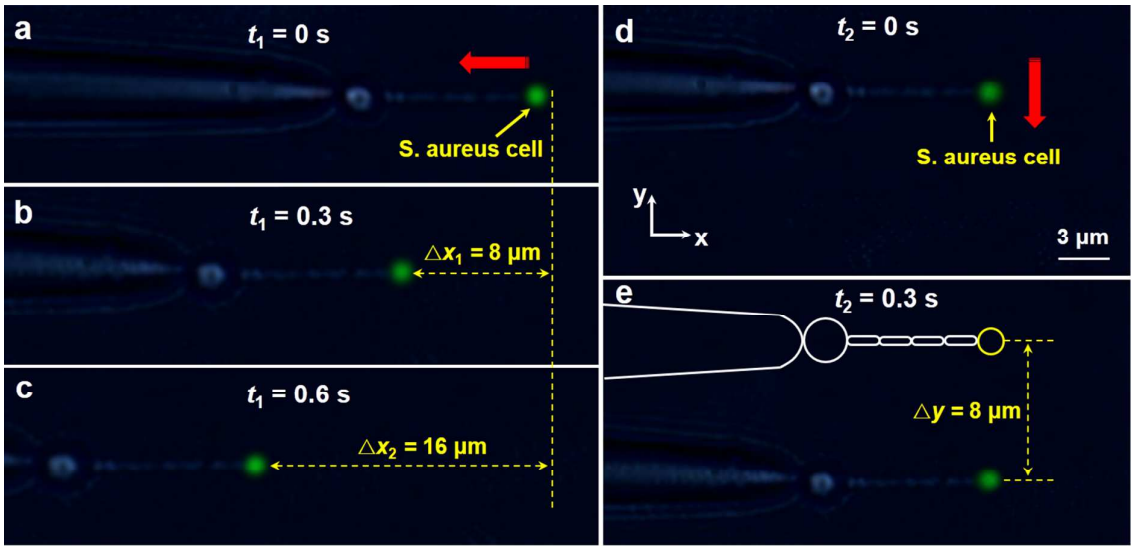

Figure S11 | Optical manipulation of a single *S. aureus* cell with the nanospear. a, At t_1 = 0 s, a *S. aureus* cell emitting green fluorescence was trapped by the nanospear. b, At t_1 = 0.3 s, the trapped *S. aureus* cell was manipulated in the $-x$ direction with a distance of 8 μm. c, At t_1 = 0.6 s, the *S. aureus* cell was further moved in the $-x$ direction with a distance of 16 μm. d, At t_2 = 0 s, the *S. aureus* cell was trapped by the nanospear. e, At t_2 = 0.3 s, the trapped *S. aureus* cell was manipulated in the $-y$ direction with a distance of 8 μm. The red arrow denotes the direction of the manipulation.

12. Light Propagation of the Nanospears with Different Deformation Angles

Using 532 nm incident light as an example, the light propagation of the nanospears with different deformation angles θ was simulated by COMSOL Multiphysics. As shown in Fig. S12, even if the deformation angle θ of the nanospear increases from 15 to 45 degrees, the incident light can still effectively propagate along the nanospear and emit a subwavelength light spot at the nanospear tip. This simulated result indicates that a certain degree of the deformability of the nanospear has no obvious influence on the scanning capabilities.

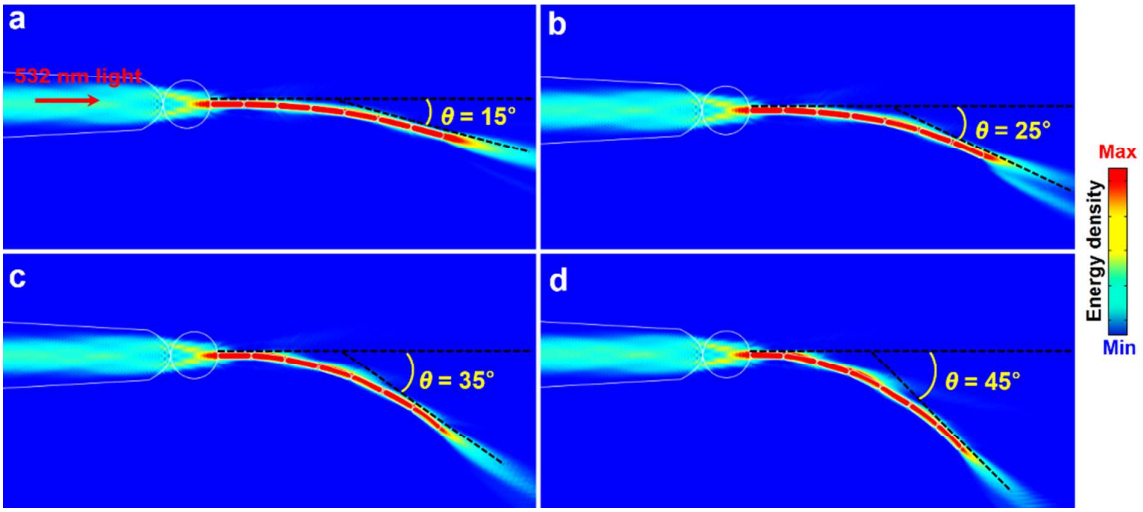

Figure S12 | Simulated energy density distributions of 532 nm incident light propagating along the nanospears with deformation angles θ of 15 (a), 25 (b), 35 (c), and 45 (d) degrees.

13. Stimulated Optical Force and Trapping Potential of the Nanospear

To demonstrate the trapping stability of the bio-nanospear, the time average optical force ($\mathbf{F}_o$) exerted on the yeast and *L. acidophilus* cells can be calculated by[6]

$$\mathbf{F}_o = \oint (\langle \mathbf{T}_M \rangle \cdot \mathbf{n})\, \mathrm{d}S\,, \tag{S7}$$

where the integration is performed over a closed surface S surrounding the cells, $\mathbf{n}$ is the unit vector, and $\langle \mathbf{T}_M \rangle$ is the time-independent Maxwell stress tensor, which can be expressed as

$$\langle \mathbf{T}_M \rangle = \frac{1}{2} \mathrm{Re}\left[\mathbf{D} \otimes \mathbf{E}^* + \mathbf{B} \otimes \mathbf{H}^* - \frac{1}{2} (\mathbf{E}^* \cdot \mathbf{D} + \mathbf{H}^* \cdot \mathbf{B}) I \right], \tag{S8}$$

where $\mathbf{E}$ is the electric field, $\mathbf{D}$ is the electric displacement, $\mathbf{B}$ is the magnetic flux field, $\mathbf{H}$ is the magnetic field, and I is the identity tensor. Because $\mathbf{F}_o$ in the y direction was the main strength to confine the cells at the optical axis and keep the shape of the bio-nanospear, we calculated the y component (F_o) of $\mathbf{F}_o$ exerted on the yeast cell and *L. acidophilus* cells as a function of the distance (D_y) between the center of the cells and the optical axis of the bio-nanospear. To further get insight into the trapping mechanism, the optical potentials (U) of the traps were also calculated by integrating F_o over the distance D

$$U = -\int F_o \, \mathrm{d}D \quad . \tag{S9}$$

The optical force F_o and trapping potential U of the yeast cell were shown in Fig. S13a. The result shows that the maximum F_o and U acted on the yeast cell were 790 pN/W and 2.3 × 10^5 k_BT/W, respectively. Furthermore, the F_o exerted on each *L. acidophilus* cell in the bio-nanospear was also calculated as a function of D_y (Fig. S13b). The result shows that the maximum F_o exerted on the first to sixth cells in the bio-nanospear were calculated to be 535, 660, 588, 490, 456, and 430 pN/W, respectively.

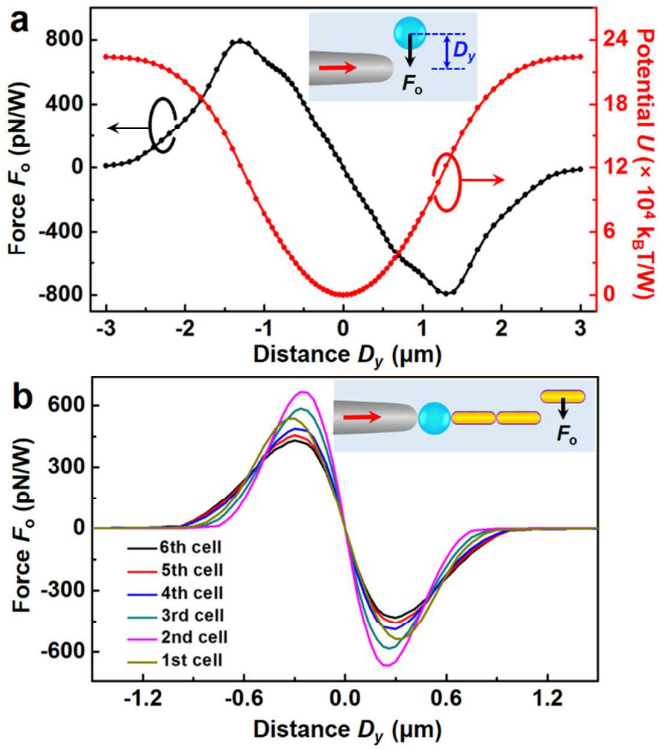

Figure S13 | Stimulated optical force and trapping potential. a, Simulated optical force F_o and trapping potential U of the yeast cell as a function of the distance D_y between the center of the cell and the optical axis of the tapered fiber in the y direction. b, Simulated F_o exerted on each *L. acidophilus* cell in the bio-nanospear as a function of D_y. Insets schematically show the calculation models.

14. Simulated Optical Intensity *versus* the Number of *L. acidophilus* Cells

Figure S14 shows the curve of the relation between the optical intensity and the number of *L. acidophilus* cells. The optical intensity was calculated by integrating the simulated intensity distribution on the surface of the *L. acidophilus* cell. It can be seen that the optical intensity along the *L. acidophilus* cell chain reaches the maximum at the second *L. acidophilus* cell and then slightly reduces for the increasing cell number.

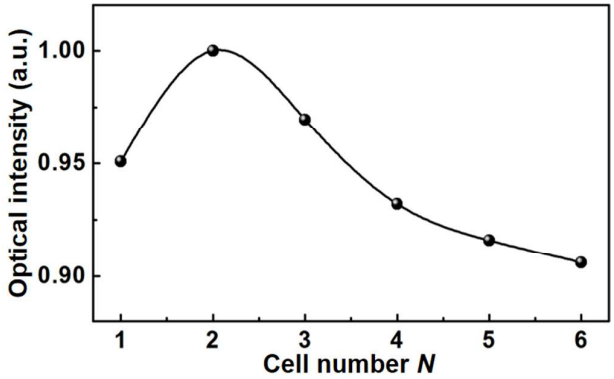

Figure S14 | Simulated optical intensity along the *L. acidophilus* cell chain as a function of the cell number N.

References

1. Borghese, F.; Denti, P.; Saija, R.; Iatì, M. A. Radiation Torque on Nonspherical Particles in the Transition Matrix Formalism. *Opt. Express* **14**, 9508–9521 (2006).
2. Gauthier, R. Theoretical Investigation of the Optical Trapping Force and Torque on Cylindrical Micro-objects. *J. Opt. Soc. Am. B* **14**, 3323–3333 (1997).
3. Neuman, K. C.; Block, S. M. Optical Trapping. *Rev. Sci. Instrum.* **75**, 2787–2809 (2004).
4. Berg-Sørensen, K.; Flyvbjerg, H. Power Spectrum Analysis for Optical Tweezers. *Rev. Sci. Instrum.* **75**, 594–612 (2004).
5. Tolić-Nørrelykke, S. F.; Schäffer, E.; Howard, J.; Pavone, F. S.; Jülicher, F.; Flyvbjerg, H. Calibration of Optical Tweezers with Positional Detection in the Back Focal Plane. *Rev. Sci. Instrum.* **77**, 103101 (2006).
6. Schmidt, B. S.; Yang, A. H.; Erickson, D.; Lipson, M. Optofluidic Trapping and Transport on Solid Core Waveguides within a Microfluidic Device. *Opt. Express* **15**, 14322–14334 (2007).